(This is a sample cover image for this issue. The actual cover is not yet available at this time.)

Computational Materials Science 54 (2012) 280–286

Contents lists available at SciVerse ScienceDirect

Computational Materials Science

journal homepage: www.elsevier.com/locate/commatsci

Dislocation morphology and nucleation within compressed Si nanospheres: A molecular dynamics study

L.M. Hale [a,*], D.-B. Zhang [b], X. Zhou [a], J.A. Zimmerman [a], N.R. Moody [c], T. Dumitrica [b,d], R. Ballarini [e], W.W. Gerberich [d]

[a] Department of Mechanics of Materials, Sandia National Laboratories, Livermore, CA 94550, USA
[b] Department of Mechanical Engineering, University of Minnesota, Minneapolis, MN 55455, USA
[c] Department of Hydrogen and Metallurgy Science, Sandia National Laboratories, CA 94550, USA
[d] Department of Materials Science, University of Minnesota, Minneapolis, MN 55455, USA
[e] Department of Civil Engineering, University of Minnesota, Minneapolis, MN 55455, USA

ARTICLE INFO

Article history:
Received 12 April 2011
Received in revised form 31 October 2011
Accepted 8 November 2011

Keywords:
Silicon
Nanoparticle
Dislocation
Molecular dynamics

ABSTRACT

Large scale molecular dynamics simulations of the compression of silicon nanospheres were performed with the Stillinger–Weber potential. Several defects were observed to cause the yielding, including dislocations, stacking faults and phase transformations. To better investigate dislocation interactions, spheres of increasing size comprised of up to one million atoms were simulated. The morphologies of the defects and the conditions under which they are formed are explored. A new and interesting route to dislocation formation is identified and examined in which perfect dislocations form on {1 1 0} planes as opposed to the expected {1 1 1} planes. The dislocations on {1 1 0} planes are observed to form through a pathway with an intermediate metastable state corresponding to a change in the atomic bonding. Density Functional based Tight Binding calculations reveal the feasibility of this pathway although the appearance of dislocations on the {1 1 0} plane in the molecular dynamics simulations is specific to the Stillinger–Weber potential.

1. Introduction

The complex loading associated with the compression of silicon nanospheres presents a situation where both phase transformation [1] and dislocation nucleation [2] are conceivable. Identifying the yielding mechanism is critical in understanding the high hardness values obtained during compression of these particles [2–5]. However, no conclusive experimental evidence for the presence of either yielding mechanism within the nanospheres has been obtained.

Molecular dynamics simulations offer a unique opportunity of investigating the possible mechanisms at the atomic level to help interpret the experimental results. However, the available interatomic potentials for silicon have various strengths and limitations, and can favor different yielding mechanisms. By investigating multiple potentials, insight can be gained into a variety of different yielding mechanisms. Comparing the simulated results with experiments can then reveal which of the simulated yielding mechanisms produces the best representation.

Previous works simulating the yielding behavior within silicon nanospheres have relied on the Tersoff potential [1,6]. The Tersoff potential was initially developed to accurately represent the high phase transformations of silicon [7–9]. As such, these previous works focused on investigating the influence of the diamond cubic to β-Sn phase transformation. Dislocations were also observed, but only for systems 20 nm in diameter or larger. Few dislocations were observed preventing any analysis of the effect of dislocation interactions.

The work presented here uses the Stillinger–Weber potential, and therefore offers an alternative description of the yielding. The Stillinger–Weber potential [10] has been shown to be superior at representing the shearing behavior and generalized stacking fault energies for silicon to the Tersoff [7,8] and EDIP [11] potentials at low temperature for shuffle set dislocations [12]. However, the Stillinger–Weber potential overestimates the energy barrier for the high pressure phase transformation of diamond cubic to β-Sn. These factors lead to the Stillinger–Weber potential favoring dislocation related yielding. Hence, the Stillinger–Weber potential may enable dislocation yielding mechanisms and interactions to be studied with smaller simulations than the Tersoff potential.

Recent papers investigating the compression of silicon nanostructures using the Stillinger–Weber potential include Fang et al. [13], who studied the compression of Si cubes and noted a

* Corresponding author. Address: PO Box 969, MS 9403, Livermore, CA 94551-0969, USA. Tel.: +1 925 294 3825; fax: +1 925 294 3410.
E-mail address: lmhale@sandia.gov (L.M. Hale).

0927-0256/$ - see front matter © 2011 Elsevier B.V. All rights reserved.
doi:10.1016/j.commatsci.2011.11.004

size dependent maximum hardness with a 10 nm side length producing the largest hardness. Only amorphous damage was reported within the cubes for the loads considered. Also, Yang et al. [14] reported for [1 0 0] oriented nanowires in compression that slip occurred on the {1 1 0} family of planes as opposed to the {1 1 1} type observed in tension.

The first part of this paper explores and discusses the observed dislocation based yielding events that occur during compression of Si nanospheres using the Stillinger–Weber potential. This reveals possible alternative yielding mechanisms than what has been previously reported with the Tersoff potential. The next section is an in-depth analysis of the process related to formation of dislocations on {1 1 0} planes and how it relates to the BCT5 compressed phase, a body-centered-tetragonal structure where every atom has a coordination number of 5 [15]. Quantum-based Density Functional based Tight Binding (DFTB) simulations reveal the {1 1 0} nucleation pathway is feasible but not favored.

2. Computational procedure

All molecular dynamics calculations were performed using the LAMMPS molecular dynamics simulation code [16] with a timestep of 1 fs. A modified version of the Stillinger–Weber potential was used where the energy is scaled to better match the bulk cohesive energy [9]. Results presented here were compared with results using the original parameters and similar yielding and plasticity behaviors were observed. The only noticeable difference found was that the modified potential has elastic properties 6.8% stiffer than the original potential due to the change in the cohesive energy. Because only the scale of the energy is changed, all observed yielding behaviors are expected to remain consistent with results from the original potential.

Three sphere sizes are presented here with 10, 20 and 34 nm diameters (26,167, 209,121, and 1,027,987 atoms respectively). The 10 nm and 20 nm spheres were analyzed at 0 and 300 K using a Nosé/Hoover temperature thermostat [17], while the 34 nm sphere was only studied at 300 K. All spheres were compressed along the [1 0 0] crystal direction. The 10 nm sphere was also compressed along the [0 1 1] and [1 1 1] directions in separate simulations. Initial sphere creation was done by generating all of the perfect bulk crystal lattice positions within a geometrically defined sphere.

Two planar indentation potentials were used to compress the spheres, one placed above the sphere (related to the direction of the y-axis) and the other equidistant below. This potential applies a force onto atoms according to their coordinates as given by

$$F_y(y) = ck(y - y_i)^2 \tag{1}$$

where F_y is the force in the y direction that the indenter applies onto each atom, k is a constant (taken to be 10.0 eV/Å), y is the y-coordinate for that atom, and y_i is the y-coordinate of the indenter. To insure that both indenters apply a repulsive force when they contact the sphere, for the upper indenter $c = -1$ when $y \geqslant y_i$ and $c = 0$ when $y < y_i$, whereas for the lower indenter $c = 1$ when $y \leqslant y_i$ and $c = 0$ when $y > y_i$. Summing this force value over all atoms provides the total load that each indenter applies onto the sphere.

Both indenters were prescribed inward velocities of 0.003125 Å/ps, resulting in a total displacement rate that is double this value for all sphere sizes except for the 34 nm diameter. The rate for the 34 nm diameter sphere was doubled to reduce the total computational time required for the simulation. The indenters were allowed to compress the spheres until an engineering compressive strain (total displacement/diameter) between 0.4 and 0.6 before the spheres were unloaded at the same rate. During compression, the linear and rotational momenta of the total sphere were subtracted from each atom to prevent the sphere from rotating and drifting before and during compression.

A number of analysis parameters were used to identify and track the phase transformations and dislocation movements. Dislocation activity was monitored with the slip vector parameter [18]. Phase identification was aided using the angular parameter [6].

$$\frac{1}{N_b}\sum_{j=1}^{N}\sum_{k=j+1}^{N}(\cos\theta_{ijk} - \cos\theta_{DC})^2 \tag{2}$$

where N is the number of nearest neighbors of atom i, θ_{ijk} is the angle between nearest neighbor bonds from atoms i, j and i, k, θ_{DC} is the bond angle for bulk diamond cubic, and N_b is the number of bond angles that have been summed over. This angular parameter is dependent on each atom's coordination number, but is advantageous as it also depends on the bonding structure around the atoms. For the work presented here, it offers an additional criterion that can help distinguish between atoms with BCT5 bonding (angular = 0.12) and other five coordinated atoms, such as those that can appear around a dislocation core (angular = 0.13–0.15) or other defect.

3. Results and discussion

3.1. Plasticity mechanisms

Compression along the [1 0 0] direction showed the formation and propagation of numerous full ½ ⟨1 1 0⟩ dislocations within the spheres. Dislocation loops would homogeneously nucleate on the {1 1 0} type planes 45° from the applied loading in the region just below the contact area. Further loading would see the front of the dislocation loop continuing to move along the {1 1 0} plane with mostly edge character, while the sides of the loop would cross slip to the more crystallographically favored shuffle set {1 1 1} planes. This resulted in the slipped planes forming a "V" shape as the dislocations proceeded diagonally through the sphere to the surface on two {1 1 1} planes connected by a {1 1 0} plane (Fig. 1). Upon reaching the surface of the sphere, the dislocations were able to terminate resulting in visible surface steps.

The "V" shaped dislocations have a few characteristics that clash with previous dislocation studies in silicon. Most predominately is the dislocation nucleation occurring on the {1 1 0} planes, which is addressed in depth in the next section. In addition to this are the facts that the dislocations are observed to nucleate at 0 K, and the resulting character of the dislocation loops is mixed and not uniform. Dislocations are seen at both 0 K and 300 K in nearly similar capacities as the main driving force behind the nucleation is the high shear stresses occurring near the indenter contact. These shear stresses approach the theoretical shear strength of the crystal and allow for geometrically necessary dislocations to nucleate homogeneously within the spheres. Thus the nucleation is stress driven and thermal activation is not necessary. The fact that the dislocation initially forms as a loop requires that the character of the dislocation must vary between different points along the line. The initial edge component must remain on the {1 1 0} plane, while the screw components are allowed to cross slip onto {1 1 1} planes. Once on the {1 1 1} planes, the dislocation line is curved, but still favors the expected pure screw and 60° orientations (Fig. 2).

While dislocations were the primary yielding mechanism for the [1 0 0] compression orientation they were not the only yielding mechanism observed as regions of BCT5 were formed. The BCT5 phase was first proposed by Boyer et al in 1991 [15]. Initially identified using the Stillinger–Weber potential and first principle calculations, BCT5 was found to be stable for certain stress states with the Stillinger–Weber results, while the first principle pseudo po-

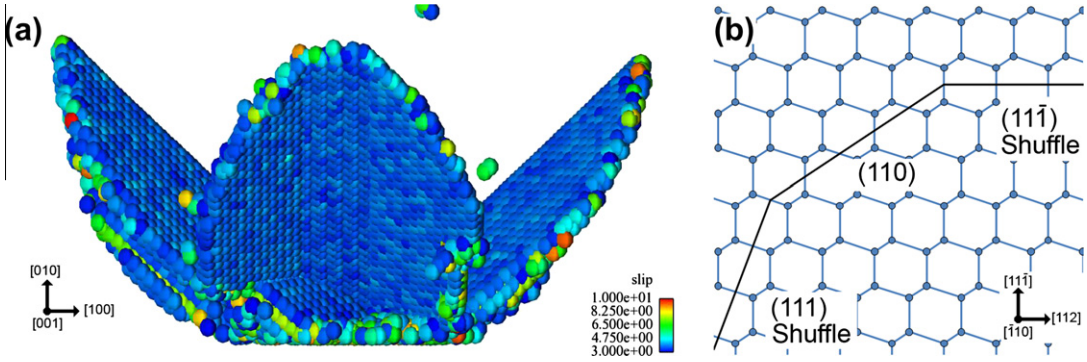

Fig. 1. Slip vector images from the 20 nm diameter radius spheres compressed at 300 K. The visible planes are ones that have slipped due to a dislocation that had traveled on that plane. The dislocation loops were seen to have traveled on at least two {1 1 1} planes connected by {1 1 0} planes.

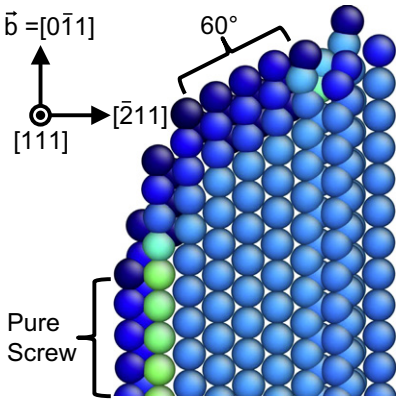

Fig. 2. Slip vector map of a (1 1 1) plane containing part of a dislocation. The dislocation core is at the left/upper edge of the colored plane showing a mixed character, but tendency towards a pure screw or 60° orientation. The dislocation crosses to a (0 1 1) plane at the right hand side of the image.

tential indicated BCT5 as metastable at all pressures. BCT5 can also be obtained through a distortion of the DC lattice [19]. One simple way of looking at this distortion is taking a glide set of [1 1 1] planes in the DC structure consisting of two planes with 2-D hexagonal structure positioned together such that each atom is neighboring three atoms in the other plane, then deforming both planes to a square lattice resulting in an additional atomic bond for each atom (Fig. 3).

The simulation of the 10 nm sphere compressed at 0 K featured the most prevalent BCT5, which is shown in Fig. 4. Atoms identified as having bonding consistent with BCT5 were shown to form in two distinct shapes: a conical structure and a highly directional region. The conical BCT5 region is seen to form within the high stress

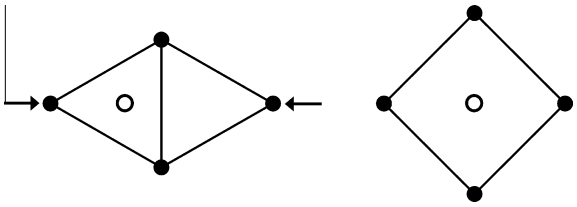

Fig. 3. A diagram allowing for a visualization of how diamond cubic silicon can transform to BCT5 upon loading. (a) The relative positions of atoms within two neighboring [1 1 1] planes in silicon of the glide set. Each atom is bound to three atoms in the other [1 1 1] plane shown, and one atom directly above/below in another plane and (b) the planes are deformed from the hexagonal packing to the square structure resulting in each atom gaining a neighbor.

regions near one of the contact areas and forms as a volume as might be expected for a high pressure phase transformation. The conical region of BCT5 remained throughout the compression and subsequent unloading. In contrast, the directional region is composed of subsequent {1 1 0} planes that have been sheared. This builds up a region consistent with BCT5 plane by plane. At higher stresses, full dislocations nucleated from the edge of the directional BCT5 region and grew to the surface. Further increases in the displacement resulted in that particular BCT5 region disappearing. An in depth discussion of the formation of the BCT5 regions and how they relate to the dislocations nucleating on the {1 1 0} planes is addressed in Section 3.2.

Compression along the [1 1 0] direction shows the formation of a wedge shaped yield zone just within the sphere near both of the compression zones that appears to be a complex region of partial dislocations, BCT5 and amorphous silicon. Continued loading shows that partial dislocations nucleate and connect the wedge shaped regions at the top and bottom that quickly transforms into a stacking fault (Fig. 5). With further deformation, the stacking fault remains and grows slightly while the wedge-shaped regions quickly decompose into purely amorphous zones.

For the third direction tested, the [1 1 1] direction showed both dislocation and stacking fault behavior. Initially, dislocations would form at the contact points and grow into the material. But rather than traveling all the way to the sphere's edge, the dislocation line would transform into a stacking fault that connected to the surface that the dislocation had originated from (Fig. 6a). At higher displacements, full dislocations would originate from this slipped region and proceed all the way to the opposite side and outside of the sphere (Fig. 6b).

When compared to the previous results using the Tersoff potential [6], some major differences are observed. For 300 K simulations, dislocation behavior was observed even in spheres as small as 5 nm with the Stillinger–Weber potential. In contrast, the Tersoff results indicated a critical size for dislocation nucleation between 10 and 20 nm in diameter below which no dislocations form. In addition, no dislocations were seen to nucleate at 0 K for the Tersoff potential, but they still readily formed for the Stillinger–Weber potential. This shows that for the study of dislocations, the Stillinger–Weber-potential has the distinct advantage over the Tersoff potential in silicon nanoparticles because smaller, less computationally expensive spheres readily show dislocation yielding.

3.2. Dislocation nucleation on {1 1 0} planes

Nucleation of the observed full dislocations during the [1 0 0] sphere compressions were seen to originate on {1 1 0} type planes. An examination of the {1 1 0} planes just prior to dislocation nucleation revealed the formation of an intermediate slip band. This slip

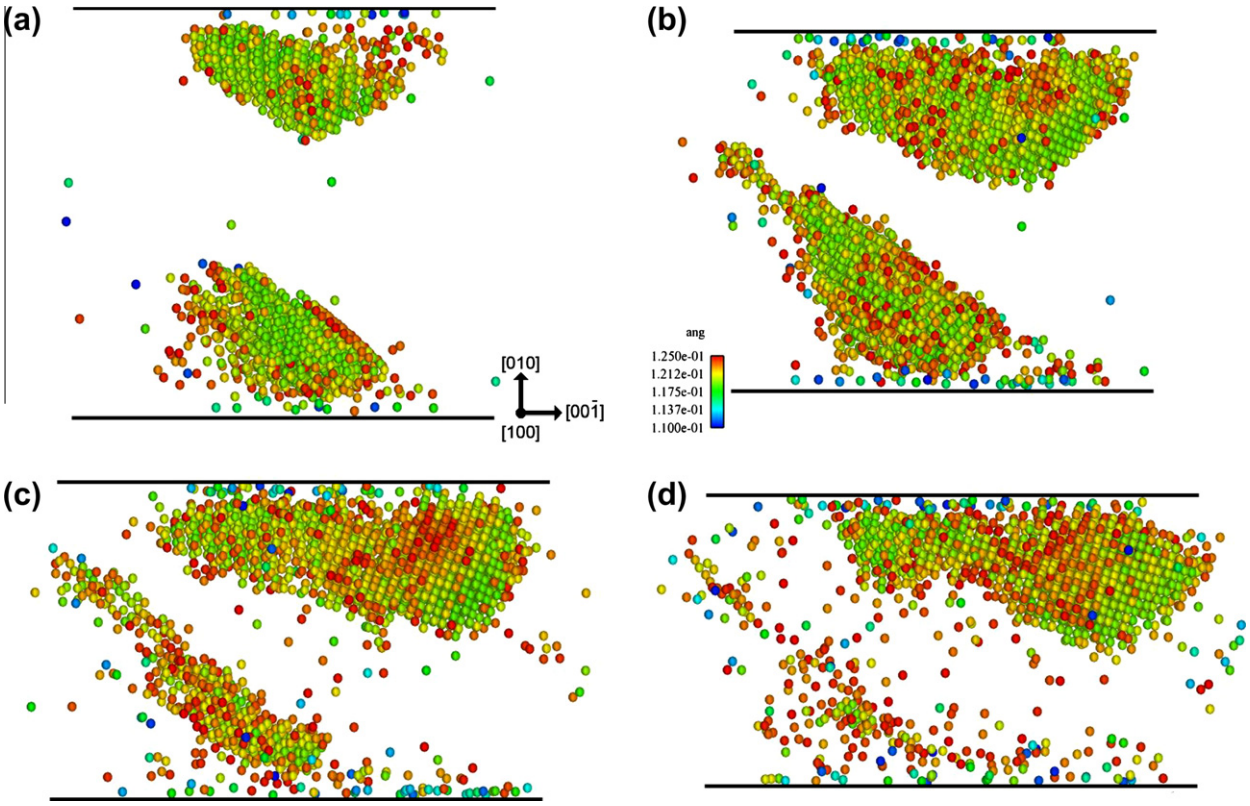

Fig. 4. Images showing the BCT5 yielding behavior seen at 0 K for compression along the [1 0 0] direction within a 10 nm diameter sphere. Lines have been added showing the positions of the indenters. The applied displacement increases from (a) to (d) with respective displacements of 2.06, 3.09, 3.86 and 4.39 nm. In (a), two distinct morphologies of BCT5 are seen: conical (top) and directional (bottom). As the load increases, the conical region is seen to expand and move off center while the directional region first grows and then disappears as it is replaced by full dislocations.

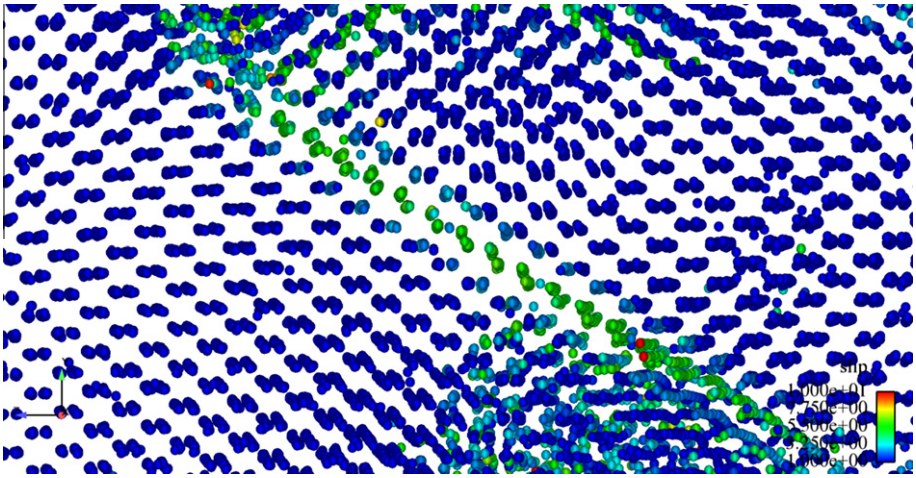

Fig. 5. A cross-section of a [1 1 0] compressed Stillinger–Weber sphere clearly showing a stacking fault.

band is visible as a plane of atoms in many of the characterization methods by having a slip vector value between 1 and 3 Å, an angular value around 0.13 and a coordination number of 5. Interestingly enough, these same values correspond to the regions identified as BCT5. This suggested that the two observed behaviors are not independent of each other and thus required a more in depth look.

In order to examine the intermediate slip that occurs prior to the nucleation of the full dislocations, a set of $(0\bar{1}1)$ planes from the 20 nm sphere compressed at 0 K were identified as having a region that slipped with respect to each other and this region was visually isolated from the bulk material. Images (Fig. 7) were taken normal to the atomic planes prior to the intermediate slip, after the slip, and finally after further slip that resulted in the formation of the full dislocation at the edge of this region. Comparing the first and last images to each other, it can be seen that the dislocation is perfect and the slip occurred in the [0 1 1] direction. Analyzing the atomic positions revealed that the resulting dislocation had the expected burgers vector of a/2 [0 1 1]. As for the intermediate step, it appears that the two planes are approximately halfway between the two end positions giving a slip of roughly a/4 [0 1 1]. Crystallographically no stable stacking fault is expected for this slip position.

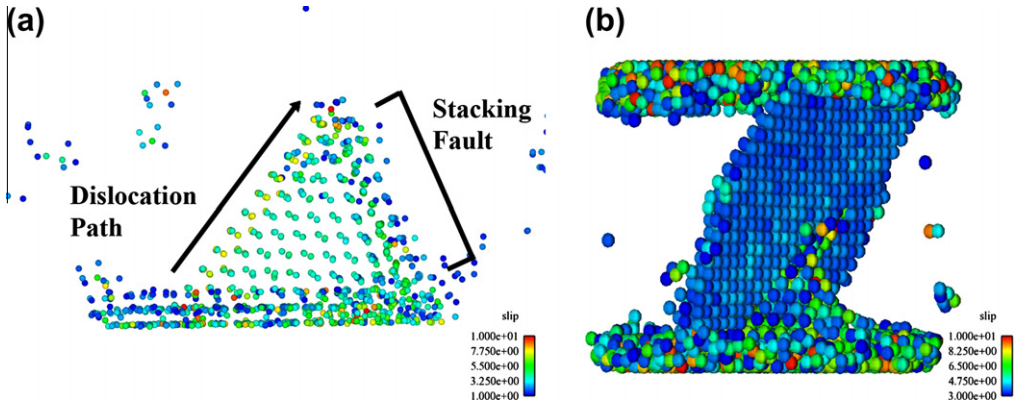

Fig. 6. The dislocation behavior for [1 1 1] compression. (a) At low loads, a dislocation forms at the contact region and grows into the crystal and transforms into a stacking fault connecting the slipped region back to the amorphous contact area and (b) higher loading results in the appearance of full dislocations that travel to the opposite surface.

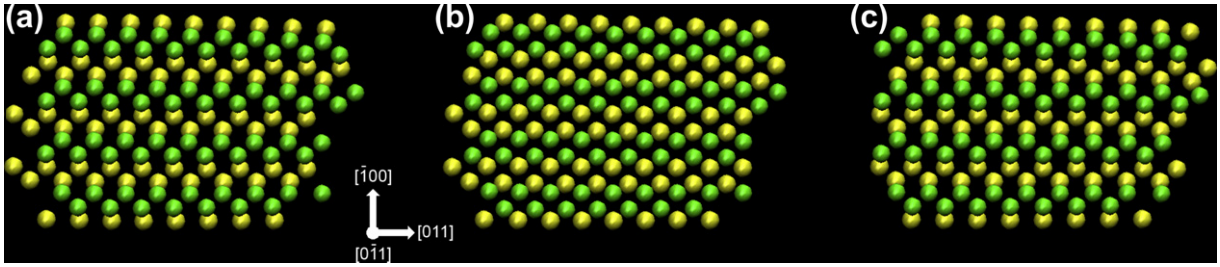

Fig. 7. A region of two neighboring $(0\bar{1}1)$ planes extracted from the compressed sphere. (a) This image shows the planes prior to any slip occurring with all atoms consistent with the DC structure. (b) Increased loading resulted in this intermediate slip of approximately a/4 [0 1 1] between these two planes. This state remains stable for a number of imaged steps. (c) Slip between the planes continues at higher loads resulting in the region returning to the DC structure. As the two planes in this region have been displaced exactly a/2 [0 1 1] from their initial positions in (a), a perfect dislocation is formed at the edge of the region.

The fact that this intermediate state is stable for a number of timesteps suggests that it corresponds to a local energy minimum. To better quantify this, a generalized stacking fault (GSF) curve was calculated for slip between pairs of {1 1 0} planes and compared to the GSF curve for shuffle set {1 1 1} slip. This was accomplished with MD simulations in which incremental slip was applied between a pair of slip planes along the slip direction. The systems were designed according to the work done by Godet et al. [12] such that the normal to the slip plane is oriented along the *x*-axis, periodic conditions are applied in the *y*- and *z*-directions and the system size is chosen to be just large enough to avoid issues with the periodicity and free surfaces. This resulted in systems of 2048 atoms and 61.448 Å × 30.724 Å × 21.724 Å dimensions for the {1 1 0} test and 1440 atoms and 47.0338 Å × 26.6064 Å × 23.0418 Å for the {1 1 1} test. The energy was then calculated for all of the incremental slip positions by performing a local minimization with one of two constraints imposed on the two slip planes: either by only allowing atoms to relax normal to the slip planes (*x* relaxation), or by constraining the atoms from relaxing along the slip direction (*xy* relaxation).

The resulting GSF curves calculated with the Stillinger–Weber potential are show in Fig. 7a. The two relaxation methods result in similar results for the {1 1 1} shuffle set slip so only the *xy* relaxation is shown. For the {1 1 0} slip, the *x* relaxation shows the halfway point of the {1 1 0} slip to be a maximum with a magnitude greater than the maximum of the {1 1 1} slip. The *xy* relaxation results in the midpoint becoming a minimum that is lower than the {1 1 1} curve. The additional relaxation afforded by the latter method is seen to result in atomic shifts within the planes nearest the slip where the atoms shift slightly in the *y* direction, but the orientation of the slip alternates for alternating atoms. Thus, the planes as a whole are not shifting relative to each other along the *y* direction, but rather the atomic arrangement is relaxing to a new structure. As such, the *xy* relaxation is taken to be representative of the true low energy pathway for slip in this plane and direction.

The slope and maximum seen with the {1 1 0} slip are only slightly higher than what is observed with the {1 1 1} shuffle set slip. The maximum values for the {1 1 1} and {1 1 0} slip measured are 0.051 and 0.058 eV/Å^2 respectively. The fact that the peak value of the {1 1 0} slip is comparable to the shuffle set slip indicates that dislocation nucleation on {1 1 0} planes to be an alternative low energy yielding path. This is indeed what is seen to occur during compressions along the [1 0 0] direction as the resolved shear stress is greatest along {1 1 0} planes.

Fig. 8a clearly shows that there exists an energy minimum at the halfway point of {1 1 0} slip. However, it does not explain why the intermediate state should be energetically favorable. The answer is obtained by a close examination of the atoms between the two planes. When the crystal is sheared the coordination of the atoms increases to 5, the atoms reconfigure to match with the bonding observed for the BCT5 structure. In terms of crystallography, it would be incorrect to call it a region of BCT5 as it only occurs on two neighboring atomic planes, but at least locally the bonding around each atom in those two planes is the same as in the BCT5 regions.

From the analysis above, it can be proposed that the intermediate slip seen is a low energy yielding mechanism for the Stillinger–Weber potential at low temperatures and can lead to the formation of either BCT5 regions or the nucleation of dislocations. Once part of a plane has undergone this intermediate slip, further loading can result in more yielding to occur. If neighboring planes yield by this intermediate slip, then the region quickly develops into a volume of BCT5. On the other hand, if the slip continues on the same plane as the original slip, then the atoms will jump to the next perfect

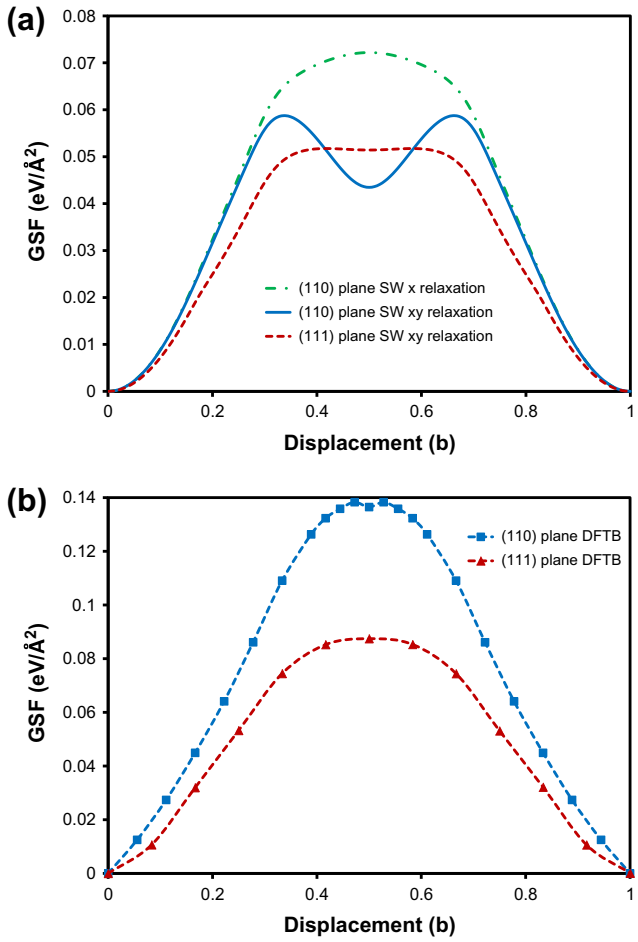

Fig. 8. The generalized stacking fault curves for ⟨1 1 0⟩ slip in Si. (a) Using the Stillinger–Weber potential, the normal GSF curve obtained by relaxing atoms only in the direction normal to the slip plane reveals no minimum for {1 1 0} planar slip. After allowing for relaxation normal to the slip direction, there is a clear energy minimum at the halfway point for slip on {1 1 0} planes corresponding to a structural change within the planes. This results in the GSF energies of {1 1 0} planes being comparable to slip those of {1 1 1} shuffle set planes and (b) quantum mechanical calculations using DFTB reveal that there is a slight minimum, but the large difference between the maximum energies makes (1 1 1) shuffle set slip much more favorable.

crystalline sites forming a full dislocation on {1 1 0} planes. While the exact stress conditions in the region of yield play the largest part in determining which behavior will occur, it is reasonable that increasing the temperature will make dislocations more favorable than BCT5 as there is a smaller energy well around the intermediate position than the crystallographic position.

It is interesting to note that slip on {1 1 0} planes was also reported for [1 0 0] Stillinger–Weber Si nanowires in compression [14]. This indicates that the {1 1 0} dislocations are not limited to nanospheres and may occur in any structures where the resolved shear stress on the {1 1 0} planes is larger than the resolved shear stress acting on {1 1 1} planes. Interestingly, only shuffle-set dislocations were observed with the Stillinger–Weber nanowires in tension. The {1 1 0} pathway may favor having a compressive pressure in the highly stressed regions.

To better investigate this novel dislocation nucleation pathway, similar GSF curves were also calculated using quantum mechanical molecular dynamics. These simulations used the DFTB [20] method, as implemented in the computational package TROCADERO [21]. Different from most empirical many body potentials such as Stillinger–Weber type, DFTB treats the electrons in an explicit way allowing for a more robust and realistic representation. The DFTB calculations of the GSF curves were performed similarly to the Stillinger–Weber results with the exception that fewer atoms were used: 16 for the {1 1 1} plane and 32 for the {1 1 0} plane. This allowed for the smallest repeat units in the *y* and *z* directions while allowing for 8 and 16 planes respectively parallel to the imposed slip.

The GSF curves obtained with DFTB and *xy* relaxation are shown in Fig. 8b. The behavior of the {1 1 1} shuffle-set slip plane is consistent with what was previously reported for this slip plane [22] with the exception being that the maximum measured here of 0.087 eV/Å^2 is less than the previously reported maximum of 0.11 eV/Å^2. This can be accounted for in that here the energies were calculated by relaxing the atoms at the slip planes in the two dimensions normal to the slip direction, whereas the original calculations only relaxed normal to the slip plane. As for the {1 1 0} slip plane, a slight decrease in energy is observed at the halfway point along the slip direction. However, the maximum energy associated with slip in the {1 1 0} plane is 0.13 eV/Å^2, which is considerably larger than the energy associated with the {1 1 1} shuffle-set. As the quantum based simulations are more accurate, this suggests that the {1 1 0} nucleation is less likely than the {1 1 1} one. However, the size of the barrier indicates that the {1 1 0} nucleation is not prohibited to occur experimentally. Note also, that under large applied external strain conditions, the energetic barriers might be significantly lower than the value reported here.

The fact that the Stillinger–Weber potential favors the five coordinated structure that leads to the {1 1 0} dislocation nucleation means that the potential as a whole probably overestimates the likelihood for homogeneous dislocation nucleation. This, along with the lack of the β-Sn phase transformation calls for caution in interpreting the results. However, this favoritism of dislocation yield also means that it could allow for the study of dislocation interactions in systems of this type with much smaller and computationally less intense simulations than other silicon potentials.

4. Summary

Molecular dynamics simulations using the Stillinger–Weber potential of compressed silicon nanospheres reveal extensive dislocation and dislocation related yielding behaviors. Depending on the orientation, dislocations are seen to nucleate near the contact points and grow on both {1 1 0} and {1 1 1} type planes. In addition, stacking faults and regions of BCT5 are also seen to occur. The extensive presence of the dislocations within the sphere sizes simulated here show that the Stillinger–Weber potential offers the opportunity to efficiently study dislocations in nanostructures of silicon with MD.

The unexpected presence of dislocations on {1 1 0} planes is investigated. By estimating the energy barrier for dislocation nucleation with generalized stacking fault calculations, it was shown that for the Stillinger–Weber potential, the barrier on {1 1 0} planes is comparable to the barrier on {1 1 1} shuffle-set planes. The low energy of the {1 1 0} slip was attributed to the presence of a metastable state along the slip pathway in which the atoms form BCT5-like bonding. A comparative study using DFTB simulations showed the barrier of the {1 1 0} slip to be considerably larger than that of the shuffle-set, indicating caution.

Acknowledgments

This work was partially supported (RB and LMH) by the National Science Foundation Grant NSF_CMMI 0800896. One of us (WWG) would like to acknowledge additional support of the Air Force through an AOARD-08-4131 program dedicated to understanding plasticity and fracture in hard materials and the Abu Dha-

bi-Minnesota Institute for Research Excellence (ADMIRE); a partnership between the Petroleum Institute (PI) of Abu Dhabi and the Department of Chemical Engineering and Materials Science of the University of Minnesota. TD and WWG thank NSF Grand No. CMMI-1000415. Additionally, four of us (LMH, XZ, JAZ, and NMR) were supported by Sandia, Livermore. Sandia National Laboratories is a multi-program laboratory managed and operated by Sandia Corporation, a wholly owned subsidiary of Lockheed Martin Corporation, for the US Department of Energy's National Nuclear Security Administration under contract DE-AC04-94AL85000.

References

[1] P. Valentini, W.W. Gerberich, T. Dumitrica, Phys. Rev. Lett. 99 (2007) 175701.
[2] W.W. Gerberich, W.M. Mook, C.R. Perrey, C.B. Carter, M.I. Baskes, R. Mukherjee, A. Gidwani, J. Heberlein, P.H. McMurry, S.L. Girshick, J. Mech. Phys. Sol. 51 (2003) 979.
[3] W.W. Gerberich, W.M. Mook, M.J. Cordill, C.B. Carter, C.R. Perrey, J.V. Heberlein, S.L. Girshick, Int. J. Plasticity 21 (2005) 2391.
[4] J. Deneen, W.M. Mook, A. Minor, W.W. Gerberich, C.B. Carter, J. Mater. Sci. 41 (2006) 4477.
[5] J.D. Nowak, A.R. Beaber, O. Ugurlu, S.L. Girchick, W.W. Gerberich, Scripta Mater. 62 (2010) 819.
[6] L.M. Hale, X. Zhou, J.A. Zimmerman, N.R. Moody, R. Ballarini, W.W. Gerberich, Comput. Mater. Sci. 50 (2011) 1651.
[7] J. Tersoff, Phys. Rev. B 37 (1988) 6991.
[8] J. Tersoff, Phys. Rev. B 38 (1988) 9902.
[9] H. Balamane, T. Halicioglu, W.A. Tiller, Phys. Rev. B 46 (1992) 2250.
[10] F.H. Stillinger, T.A. Weber, Phys. Rev. B 31 (1985) 5262.
[11] M.Z. Bazant, E. Kaxiras, J.F. Justo, Phys. Rev. B 56 (1997) 8542.
[12] J. Godet, L. Pizzagalli, S. Brochard, P. Beauchamp, J. Phys.: Condens. Matter 15 (2003) 6943.
[13] K.C. Fang, C.I. Weng, S.P. Ju, J. Nanopart. Res. 11 (2009) 581.
[14] Z. Yang, Z. Lu, Y.P. Zhao, J. Appl. Phys. 106 (2009) 023537.
[15] L.L. Boyer, E. Kaxiras, J.L. Feldman, J.Q. Broughton, M.J. Mehl, Phys. Rev. Lett. 67 (1991) 715.
[16] LAMMPS Molecular Dynamics Simulator. <http://lammps.sandia.gov/>.
[17] W.G. Hoover, Phys. Rev. A 31 (1985) 1695.
[18] J.A. Zimmerman, C.L. Kelchner, P.A. Klein, J.C. Hamilton, S.M. Foiles, Phys. Rev. Lett. 87 (2001) 165507.
[19] D.E. Kim, S.I. Oh, J. Appl. Phys. 104 (2008) 013502.
[20] Th. Frauenheim, F. Weich, Th. Köhler, S. Uhlmann, D. Porezag, G. Seifert, Phys. Rev. B 52 (1995) 11492.
[21] R. Rurali, E. Hernández, Comput. Mater. Sci. 28 (2003) 85.
[22] Y.-M. Juan, E. Kaxiras, Phil. Mag. A 74 (1996) 1367.